Structural Monitoring and Maintenance, *Vol. 11, No. 3 (2024) 219-234*
https://doi.org/10.12989/smm.2024.11.3.219

Strength reduction factor spectra based on adaptive damping of SDOF systems

Feng Wang*, Kexin Yao[a] and Wanzhe Zhang[b]

College of Civil Engineering Dalian Minzu University, Dalian Minzu University, Dalian 116600, China

(*Received March 19, 2024, Revised May 20, 2024, Accepted June 10, 2024*)

Abstract. The strength reduction factor spectrum is traditionally obtained from a single-degree-of-freedom (SDOF) system with a constant damping coefficient. However, according to the principle of Rayleigh damping, the damping coefficient matrix of a system changes with the stiffness matrix, and the damping coefficient of an equivalent SDOF system changes with the tangent stiffness coefficient. In view of that, this study proposes an equivalent SDOF system with an adaptive damping coefficient and derives a standardized reaction balance equation. By iteratively adjusting the strength reduction factor, the corresponding spectrum with an equivalent ductility factor is obtained. In addition, the ratio between the strength reduction factor that considers adaptive damping and the traditional strength reduction factor, denoted by η, is determined, and the η-μ-T relationship is obtained. Seismic records of Classes C, D, and E sites are selected as excitations. Moreover, a nonlinear response time-history analysis is performed to establish the relationship between the η and T values for the equivalent ductility factor μ. Further, by exploring the effects of the site class, ductility factor, second-order stiffness coefficient, and period T on the mean value of η, a simplified calculation equation of mean η is derived, and η is used as a modified value for the traditional strength reduction factor R spectrum.

Keywords: damping coefficient; ductility factor equivalent SDOF system; inelastic spectrum; strength reduction factor

1. Introduction

In the seismic design of structures, the concept of the strength reduction factor is presented to achieve a reasonable balance between economy and safety. Newmark and Hall (1973) first proposed the concept of the strength reduction factor. Krawinkler and Nassar (1992) and Miranda (1994) proposed various strength reduction models. Subsequently, with the development of seismic design theory and methods, a large number of studies have been conducted to study the influencing factors and applications of the strength reduction factor. Fajfar and Vidic (1994) extensively studied the influence of structural parameters on the strength reduction factor according to the non-elastic responses of single-degree-of-freedom systems to various ground motions. Lee *et al.* (1999) compared the double-linear elastoplastic strengthening model, strength

*Corresponding author, Professor, E-mail: win_0803@163.com
[a]MA. Student
[b]MA. Student

Copyright © 2024 Techno-Press, Ltd.
http://www.techno-press.org/?journal=smm&subpage=7 ISSN: 2288-6605 (Print), 2288-6613 (Online)

degradation model, stiffness degradation model, and pinching model and investigated the influences of the stiffness coefficient and stiffness degradation coefficient of a short periodic structure on the seismic force modification factor. Borzi and ElnasHai (2000) investigated the elastoplastic acceleration spectra of two hysteresis models considering the influences of seismic magnitude and structural cycles.

Recently, some researchers investigated the effects of site characteristics on strength reduction factor. He and Agrawal (2004) investigated the relations between the strength reduction factor and ductility demand of inelastic structures subjected to the near-fault ground motions based on the proposed pulse model. Ahmadi and Khoshnoudian (2015) carried out a sensitivity analysis to examine the impacts of various parameters on the strength reduction factors of the MDOF systems considering the soil-structure interaction effects. Salimbathrami and Gholhaki (2019) investigate the strength reduction factor and CR (the ratio of inelastic to elastic displacement) of SDOF under horizontal and vertical components of near and far-field earthquakes, respectively, and concluded that strength reduction factor corresponding to the near and far-field ground motions can be different, and CR does not depend on type of earthquake.

Based on the assumption of an equivalent modal SDOF system, a number of studies analyzed the modal strength reduction factors and applied them to various structural systems. Loulelis *et al*. (2018) , Muho *et al.* (2018) and Kalapodis *et al.* (2018) investigated the modal strength reduction factors of the steel moment-resisting frames RC moment-resisting frames and plane steel braced frames, respectively. Considering that the strength reduction factor is determined by an SDOF system, Gerami *et al*. (2017) discussed the effects of the high mode and an MDOF on the strength reduction factor of frame structures subjected to far and near-fault ground motions and indicated that these effects could be remarkable for near-field motions.

Currently, many researchers applied the strength reduction factor to investigate the seismic performance of various types of structures. For irregular structures, Thuat *et al.* (2020) studied the relationship between the intensity reduction coefficient and the maximum ductility coefficient, and provided an approximate equation to express their relationship, and presented the means and standard deviations of the relationship factor through the approximate equation and Monte Carlo simulations. Gamit and Amin (2021) compared the seismic performance of structures designed using direct displacement-based design and traditional seismic design through the strength reduction factor, finding that the former can more efficiently dissipate seismic energy. According to the Venezuelan seismic design code, Ramon *et al.* (2022) evaluated the strength reduction factor of low-, medium-, and high-rise RC buildings using modal response spectrum analysis and Pushover analysis, in which the influence of response reduction factor, overstrength factor, and ductility factor were considered, and the more representative value for the strength reduction coefficient was provided. Shi and wang *et al*. (2023) researched the nonlinear seismic response behavior of fused structures through the strength reduction factor spectrum, considering the interaction between the primary structure and fuses. The study analyzed the effects of yield displacement ratio, initial stiffness ratio, and ductility factor on the strength reduction coefficient, and provided a simplified equation for the strength reduction coefficient spectra with constant ductility factors.

It is generally known that structural damage during an earthquake depends not only on the amplitude of the response, such as displacement, but also on the cumulative energy dissipation, which to a certain extent relates to the ground motion duration (2020). Lu and Wei (2008) presented the damage-based strength reduction factor spectra with the constant damage index based on the modified Park and Ang model. On this basis, Zhang *et al.* (2017) studied the damage-based strength reduction factor for mainshock-aftershock sequence-type ground motions and proposed an empirical expression by regression analysis.

Consierding the multidimensional coupling characteristics of seismic excitations and reposnses of structures, based on previous theoretical foundations, Wang *et al.* (2004) proposed the concept of the inelastic response spectra for bi-directional earthquake excitations. On this basis, Wang and Li established the strength reduction factor spectra of constant ductility factors for bi-directional earthquake excitations through two methods (Wang *et al.* 2009), furthermore, presented a damage-based strength reduction factor spectra for the system subjected to bidirectional ground motions and the empirical expression and the corresponding procedure are proposed (Wang and Li 2023).

The inelastic spectrum is traditionally obtained from a SDOF system with a constant damping coefficient (Harikrishnan and Gupta 2020, Savvinos *et al.* 2022, Silva *et al.* 2023). However, according to the principle of Rayleigh damping, the damping coefficient matrix of a system changes with the stiffness matrix, and the damping coefficient of an equivalent SDOF system changes with the tangent stiffness coefficient. In view of that, this study proposes an equivalent SDOF system with an adaptive damping coefficient and derives a standardized reaction balance equation. By iteratively adjusting the strength reduction factor, the corresponding spectrum with an equivalent ductility factor is obtained. In addition, the ratio between the strength reduction factor that considers adaptive damping and the traditional strength reduction factor, denoted by η, is determined, and the η-μ-T relationship is obtained. Seismic records of Classes C, D, and E sites are selected as excitations. Moreover, a nonlinear response time-history analysis is performed to establish the relationship between the η and T values for the equivalent ductility factor μ. Further, by exploring the effects of the site class, ductility factor, second-order stiffness coefficient, and period T on the mean value of η, a simplified calculation equation of mean η is derived, and η is used as a modified value for the traditional strength reduction factor *R* spectrum.

In taditional equivalent single-degree-of-freedom (SDOF) systems, a premise is that the damping coefficient matrix of the original structure is constant. However, according to the principles of Rayleigh damping, the damping coefficient matrix changes with the instantaneous stiffness matrix of a structure. To address this challenge, this study proposes an equivalent SDOF system with an adaptive damping coefficient. In addition, the corresponding strength reduction factor R_A spectrum for an adaptively changing damping coefficient is established and compared with the traditional strength reduction factor *R* spectrum with a constant damping coefficient. Based on the comparison results, the modified value for the R spectrum is obtained.

2. Traditional strength reduction factor R spectrum with constant damping

The motion equation of a *n*-story building under horizontal ground motion is expressed as follows

$$\mathbf{M}\ddot{\mathbf{x}}(t)+\mathbf{C}\dot{\mathbf{x}}(t)+\mathbf{F}(t)=-\mathbf{MI}\ddot{x}_g(t) \tag{1}$$

where **M** is the mass matrix, **C** is the constant damping coefficient matrix, **F**(t) is the restitution force vector, **x**(t) is the displacement response vector, and the vector **I** represents the 1 × n identity matrix $[1\ 1\ \ldots\ 1]^{\mathrm{T}}$.

According to this hypothesis of inelastic modal equivalent SDOF system, **x**(t) can be expanded in terms of the natural vibration modes of the corresponding linear elastic system.

$$\mathbf{x}(t) = \mathbf{\Phi} \cdot \mathbf{d} = \sum_{i=1}^{n} \boldsymbol{\varphi}_i d_i(t) \tag{2}$$

where $\boldsymbol{\varphi}_i$ is the i-th mode shape vector and $d_i(t)$ is the linear displacement response vector. Substituting Eq. (2) into Eq. (1), employing the orthogonality of modes, the uncoupled equations can be derived as

$$\ddot{q}_i(t) + 2\xi\omega_i\dot{q}_i(t) + f_{s,i}(t) = -\ddot{x}_g(t), \quad i = 1,\cdots,n \tag{3}$$

in whichi ω_i is the natural vibration frequency, ξ is the damping ratio, the displacement response $q_i(t)$ represents $d_i(t)/\gamma_i$, where γ_i is the modal participation factors, and the resisting force $f_{s,i}(t)$ represents $F_i(t)d_i(t)/\gamma_i\boldsymbol{\varphi}_i^T\mathbf{M}\boldsymbol{\varphi}_i$, where $F_i(t)$ is the resisting forces of the i-th mode. The first mode of equivalent SDOF systems in considered, and the subscript of corresponding parameters that represents the mode order is omitted.

The instantaneous relative displacement is defined as $u(t)$, and $u(t)= q(t)/q_{yie}$, in which q_{yie} is yield displacement. The maximum value of $u(t)$ is the ductility factor μ. According to the definition of strength reduction factor [1], the following expression is given.

$$R = \frac{\max|f_e(t)|}{f_{yie}} \tag{4}$$

where $f_e(t)$ and fyie are resisting force and yield force of the elastic SDOF system, respectively. Substituting $u(t)$ and Eq. (4) into Eq. (3), the following equation can be derived by organizing.

$$\begin{cases} \ddot{u}(t) + 2\xi\omega\dot{u}(t) + \omega^2 f_{rel}(t) = -\dfrac{\omega^2 \cdot R}{\beta \cdot \mathrm{PGA}} \cdot \ddot{x}_g(t) \\ s.t. \quad \max|u(t)| = \mu \end{cases} \tag{5}$$

where β is the earthquake amplification factor, PGA is the peak ground acceleration, and $f_{rel}(t)$ is the instantaneous relavtive seismic force, and $f_{rel}(t)=f_s(t)/f_{yie}$.

3. Improved strength reduction factor R_A spectrum with adaptive damping

3.1 R_A spectrum model

It should be noted that Eq. (1) is established under the premise of a constant damping coefficient matrix. However, in the plastic deformation stage, the stiffness softens locally or in the whole structure, and the modal damping ratio changes accordingly; thus, matrix **C** in Eq. (1) changes with the stiffness matrix. Therefore, in this study, the damping coefficient matrix **C** is replaced by an adaptively changing, instantaneous damping coefficient matrix $\boldsymbol{C}(t)$. Accordingly, Eq. (1) can be rewritten as follows:

$$\mathbf{M}\ddot{\mathbf{x}}(t)+\mathbf{C}(t)\dot{\mathbf{x}}(t)+\mathbf{F}(t) = -\mathbf{MI}\ddot{x}_g(t) \tag{6}$$

After the derivation, it can be written that

$$\ddot{q}(t) + 2\xi\omega_{ins}(t)\dot{q}(t) + f_s(t) = -\ddot{x}_g(t) \tag{7}$$

Eq. (7) represents the motion equation of the modal equivalent SDOF system with adaptive damping. Different from Eq. (3), in Eq. (7), frequency ω_i is replaced by $\omega_{ins,i}(t)$. In this study, only the first mode is considered, and thus, the subscript is omitted. According to the derivation process mentioned in Section 1, the R_A spectrum with an equivalent ductility factor of an SDOF system with adaptive damping can be derived as follows

$$\begin{cases} \ddot{u}(t) + 2\xi\omega_{ins}(t)\dot{u}(t) + \omega^2 f_{rel}(t) = -\dfrac{\omega^2 \cdot R_A}{\beta \cdot \mathrm{PGA}} \cdot \ddot{x}_g(t) \\ s.t. \quad \max\left|u(t)\right| = \mu \end{cases} \tag{8}$$

Since both $\omega_{ins}(t)$ and ω appear in Eq. (8), it is necessary to pay attention to the difference between them. In addition, it should be noted that R_A is the strength reduction factor of an SDOF system with adaptive damping, and its physical meaning is the same as that of R.

3.2 R_A spectrum establishment

The specific steps of the R_A spectrum establishment process are as follows:

(1) Set a target ductility factor, denoted as μ;

(2) Set a value for the period T and substitute it into $\omega = (2\pi / T)^{0.5}$ to obtain the natural frequency;

(3) Take an initial R_A value and substitute it into Eq. (8) to calculate $u(t)$ and $\max|u(t)|$;

(4) Compare $\max|u(t)|$ with μ, and if the deviation between them meets the threshold requirement, consider that $\max|u(t)|= \mu$; then, obtain the R_A corresponding to μ and T;

(5) If the deviation between $\max|\mu_d(t)|$ and μ does not meet the threshold requirement, that is, $\max|\mu(t)| \neq \mu$, adjust R_A and repeat Steps 3–5 until the condition of $\max|u(t)| = \mu$ is satisfied. Generally, a small initial value is selected for R_A, and then it is gradually increased;

(6) Repeat Steps 2–5 using different T values to obtain the R_A spectrum corresponding to the same μ;

(7) Repeat Steps 1–6 using different μ values to obtain the R_A spectrum corresponding to different μ values.

3.3 R_A/R ratio

Recently, there have been numerous studies on the traditional R spectrum, and various R spectrum models have been developed. In this study, on the basis of the traditional R spectrum, the traditional R spectrum is modified using the R_A/R ratio as follows

$$\eta(\mu, T) = \frac{R_A(\mu,T)}{R(\mu,T)} \tag{9}$$

where η is a function of μ and T, which can be regarded as the η spectrum with an equivalent ductility factor.

According to the definition of strength reduction factor, it holds that

$$\eta\left(\mu,T\right)=\frac{R_A}{R}=\left(\frac{\mu\cdot q_{e,A,\max}}{q_{A,\max}}\right)\Bigg/\left(\frac{\mu\cdot q_{e,\max}}{q_{\max}}\right)=\frac{q_{\max}}{q_{A,\max}} \tag{10}$$

where $q_{e,max}$ and $q_{e,A,max}$ are the maximum linear elastic displacement values obtained from Eqs. (2) and (5), respectively.

In the linear elastic stage, $q_{e,max}$ = $q_{e,A,max}$, where q_{max} and $q_{A,max}$ are the maximum plastic displacements. It can be seen from Eq. (10) that with a smaller η value, the nonlinear displacement of an SDOF system with adaptive damping will be greater in comparison to the traditional SDOF system, and vice versa.

4. Ground motions and variables considered

4.1 Ground motions records considered

A total of 178 earthquake ground motions recorded for 16 different earthquakes are selected from the PEER Strong Motion Database. According to the NEHRP (2003) provisions, the selected earthquake ground motions are classified based on the average shear wave velocity and site classes, namely C—very dense soil and soft rock site (V_s=360-750 m/s), D—stiff soil site (V_s=180-360 m/s) and soft soil site (V_s < 180 m/s), respectively, listed in Tables 1-3. The selected ground motions have common characteristics as: (1) Magnitude (Ms) = 6~8; (2) distance to rupture = 15 km~45 km; (3) At least one of the two horizontal components has peak ground acceleration (PGA) ≥ 0.1 g, approximately

4.2 Variables of mean R_A and R spectra

The damping ratio of the SDOF system is set to 0.05, and the bilinear ideal elastic-plastic model is selected as the hysteretic model of the SDOF system to analyze the influence of yield stiffness coefficients on the results. Furthermore, for constructing the mean R_A, R and η spectra, the different variables are follows:

(1) The period of the SDOF system varies from 0.1 s to 5.0s with an interval of 0.1s.

(2) Five ductility capacities μ=1.5, 2, 3, 4and 6 are selected to consider different ductility performances.

(3) Seven yield stiffness coefficients α=0.02, 0.05, 0.1, 0.2, 0.3, 0.4 and 0.5 are selected to considered different stiffness degradation for hysteretic model of systems.

Due to the space limitation, only the representative results are shown in the following sections, while the other cases having similar results are not presented.

5. Mean R_A and R spectra comparison

Fig. 1 shows the R and R_A spectra with an equivalent ductility factor for different seismic site classes, where the yield stiffness coefficient α equals 0.1. As shown in Fig. 1, for both the R spectrum and the R_A spectrum, when the ductility factor is small (e.g., μ = 1.5 or 2), the plateau section of the spectrum is approximately a horizontal line. As the ductility factor increases, the plateau section of the spectra fluctuates significantly and irregularly, especially for Class C sites.

Table 1 The ground motion records for site class C

Stations	Earthquakes	Components	Stations	Earthquakes	Components
1095 Taft Lin-Coln School	Kern County (52/7/21,Ms7.4)	TAF021 TAF111	6604 Cerro Prieto	Victoria,Mexico (80/06/09,Ms6.4)	CPE045 CPE315
1652Anderson Dam	Loma Prieta (89/10/18,Ms6.9)	AND270 AND360	89324 Rio Dell Overpass-FF	Cape Mendocino (92/04/25,M7.1)	RIO270 RIO360
24157 LA-Baldwin Hills	Northridge (94/1/17,Ms6.7)	BLD090 BLD360	CHY029	Chi-Chi (99/09/20,M7.6)	CHY029-N CHY029-W
14403 LA-116th St School	Northridge (94/01/17,Ms6.7)	116090 116360	ALS	Chi-Chi (99/09/20,M7.6)	ALS-E ALS-N
24605 LA-Univ. Hospital	Northridge (94/01/17,Ms6.7)	UNI005 UNI095	CHY052	Chi-Chi (99/09/20,M7.6)	CHY052-E CHy052-N
23 Coolwater	Landers (92/06/28,Ms7.3)	CLW-LN CLW-TR	1061 Lamont	Duzce (99/11/12,M7.1)	1061-N 1061-E
6604 Cerro Prieto	Imperial Valley (79/10/15,Ms6.5)	H-CPE147 H-CPE237	Arcelik	Kocaeli (99/08/17,M7.4)	ARC000 ARC090
57504 Coyote Lake Dam	Loma Prieta (89/10/18,Ms6.9)	CLD195 CLD285	24577 Fort Irwin	Landers (92/06/28,M7.3)	FTI000 FTI090
Tcu045	ChiChi (99/09/20,Ms7.6)	TCU045-N TCU045-W	57064 Fremont-Mission San Jose	Loma Prieta (89/10/18,M6.9)	FRE000 FRE090
Tcu047	ChiChi (99/09/20,Ms7.6)	TCU047-N TCU047-W	57383 Gilroy Array#6	Loma Prieta (89/10/18,M6.9)	G06000 G06090
90021 LA-N Westmoreland	Northridge (94/01/17,Ms6.7)	WST000 WST270	58378 APEEL 7-Pulgas	Loma Prieta (89/10/18,M6.9)	A07000 A07090
CHY086	Chi-Chi (99/09/20,Ms7.6)	CHY086-N CHY086-W	58498 Hayward-BART Sta	Loma Prieta (89/10/18,M6.9)	HWB220 HWB310
286 Superstition Mtn Camera	Imperial Valley (79/10/15,Ms6.5)	H-SUP045 H-SUP135	47006 Gilroy Gavilan Coll	Morgan Hill (84/04/24,M6.2)	GIL067 GIL337
12149 Desert Hot Springs	Landers (92/06/28,Ms7.3)	DSP000 DSP090	24607 Lake Hughes #12A	Northridge (94/01/17,M6.7)	H12090 H12180
24389LA-Century City CC North	Northridge (94/01/17,Ms6.7)	CCN090 CCN360	24611 LA-Temple & Hope	Northridge (94/01/17,M6.7)	TEM090 TEM180
14403 LA-116th St School	Whittier Narrows (87/10/01,Ms6.0)	A-116270 A-116360	90020 LA-W 15th St	Northridge (94/01/17,M6.7)	W15090 W15180
90009 N Hollywood Coldwater	Whittier Narrows (87/10/01,Ms6.0)	A-CWC180 A-CWC270	90033 LA-Cypress Ave	Northridge (94/01/17,M6.7)	CYP053 CYP143

The R and R_A spectra are plotted in the same coordinate system in Fig. 2, where $\alpha = 0.2$. In Fig. 2, it can be seen that under the conditions of the same site class, α, and μ, the value of the R_A spectrum is significantly smaller than that of the R spectrum.

Table 2 The ground motion records for site class D

Stations	Earthquakes	Components	Stations	Earthquakes	Components
6621 Chihuahua	Imperial Valley (79/10/15,M6.5)	CHI012 CHI282	NST	Chi-Chi (99/09/20,M7.6)	NST-E NST-N
1695 Sunnyvale Colton Ave.	Loma Prieta (89/10/18,M6.9)	SVL270 SVL360	6622 Compuertas	Imperial Valley (79/10/15,M6.5)	H-CMP015 H-CMP285
1028 Hollister City Hall	Loma Prieta (89/10/18,M6.9)	HCH090 HCH180	36227 Parkfield Cholame 5W	Coalinga (83/05/02,M6.4)	H-C05270 H-C05360
22074 Yermo Fire Station	Landers (92/06/28,M7.3)	YER270 YER360	Iznik	Kocaeli (99/08/17,M7.4)	IZN180 IZN090
90063 Glendale Las Palmas	Northridge (94/01/17,M6.7)	GLP177 GLP267	57066Agnews State Hospital	Loma Prieta (89/10/18,M6.9)	AGW000 AGW090
90016 LA - N Faring Rd	Northridge (94/01/17,M6.7)	FAR000 FAR090	57425 Gilroy Array#7	Loma Prieta (89/10/18,M6.9)	GMR000 GMR090
90091 LA – Saturn St	Northridge (94/01/17,M6.7)	STN020 STN110	47125 Capitola	Morgan Hill (84/04/24,M6.2)	CAP042 CAP132
TCU042	Chi-Chi (99/09/20,M7.6)	TCU042-N TCU042-W	47380 Gilroy Array #2	Morgan Hill (84/04/24,M6.2)	G02000 G02090
TCU107	Chi-Chi (99/09/20,M7.6)	TCU107-N TCU107-W	24303 LA-Hollywood Stor	Northridge (94/01/17,M6.7)	HOL090 HOL360
CHY036	Chi-Chi (99/09/20,M7.6)	CHY036-N CHY036-W	24309 Leona Valley #6	Northridge (94/01/17,M6.7)	LV6090 LV6360
6605 Delta	Imperial Valley (79/10/15,M6.5)	H-DLT262 H-DLT352	90034 LA-Fletcher Dr	Northridge (94/01/17,M6.7)	FLE144 FLE234
CHY010	Chi-Chi (99/09/20,M7.6)	CHY010-E CHY010-N	90054 LA-Centinela St	Northridge (94/01/17,M6.7)	CEN155 CEN245
CHY034	Chi-Chi (99/09/20,M7.6)	CHY034-E CHY034-N	12025Palm Springs Airport	N.Palm Springs (86/07/08,M6.0)	PSA000 PSA090
CHY046	Chi-Chi (99/09/20,M7.6)	CHY046-N CHY046-W	994 Gormon Oso Pump Plant	San Fernando (71/02/09,M6.6)	OPP000 OPP270
Atakoy	Kocaeli (99/08/17,M7.4)	ATK000 ATK090	135 LA-Hollywood Stor Lot	San Fernando (71/02/09,M6.6)	PEL090 PEL180
Bolu	Duzce (99/11/12,M7.1)	BOL000 BOL090	6621 Chihuahua	Victoria (80/06/09,Ms6.4)	CHI102 CHI192
El Centro Array#1	Imperial Valley (79/10/15,M6.5)	H-E01140 H-E01230	90003 Northridge-Saticoy St	Whittier Narrows (87/10/01,M6.0)	A-STC090 A-STC180
5061Calipatria Fire State	Imperial Valley (79/10/15,M6.5)	H-CAL225 H-CAL315			

Table 3 The ground motion records for site class E

Stations	Earthquakes	Components	Stations	Earthquakes	Components
5057 El Centro Array #3	Imperial Valley (79/10/15,M6.5)	H-E03140 H-E03230	CHY002	Chi-Chi (99/09/20,M7.6)	CHY002-E CHY002-N
1002 APEEL 2-Redwood City	Loma Prieta (89/10/18,M6.9)	A02043 A02133	CHY008	Chi-Chi (99/09/20,M7.6)	CHY008-E CHY008-N
9001 Montebeel-B R	Northridge (94/1/17,M6.7)	BLF206 BLF296	CHY025	Chi-Chi (99/09/20,M7.6)	CHY025-N CHY025-W
58117 Treasure Island	Loma Prieta (89/10/18,M6.9)	TRI000 TRI090	CHY039	Chi-Chi (99/09/20,M7.6)	CHY039-N CHY039-W
0 Shin-Osaka	Kobe (95/01/16,M6.9)	SHI000 SHI090	CHY041	Chi-Chi (99/09/20,M7.6)	CHY041-N CHY041-W
0 Kakogawa	Kobe (95/01/16,M6.9)	KAK000 KAK000	CHY092	Chi-Chi (99/09/20,M7.6)	CHY092-E CHY092-N
Ambarli	Kocaeli (99/08/17,M7.4)	ATS000 ATS090	CHY107	Chi-Chi (99/09/20,M7.6)	CHY107-E CHY107-N
TCU117	Chi-Chi (99/9/20,M7.6)	TCU117-N TCU117-W	TCU040	Landers (92/06/28,M7.3)	TCU040-N TCU040-W
TCU118	Chi-Chi (99/9/20,M7.6)	TCU118-N TCU118-W	TCU111	Loma Prieta (89/10/18,M6.9)	TCU111-N TCU111-W
CHY104	Chi-Chi (99/9/20,M7.6)	CHY104-E CHY104-N	TCU115	Chi-Chi (99/09/20,M7.6)	TCU115-N TCU115-W

There have been many studies on the traditional *R* spectrum. By analyzing the ratio between the mean R_A spectrum and the mean *R* spectrum, i.e., the η spectrum, the traditional *R* spectrum is modified in this study.

6. Analysis of ration between R_A and *R* spectra

6.1 Mean η Spectrum

Fig. 3 shows the mean η spectrum with an equivalent ductility factor for different values of yield strength coefficient α, which is used to analyze the effects of μ and T on η. In the analysis, the value of α was set to 0.1, 0.3, and 0.5, in turn. The value of parameter μ in the η spectrum was set to 1.5, 2, 3, 4, and 6, in turn. Fig. 4 shows the mean η spectrum with the constant yield stiffness coefficient for different ductility factor values, which was mainly used to analyze the effects of α and T on η. The values of μ were 1.5, 3, and 6, and the values of α in the η spectrum were 0.1, 0.2, 0.3, 0.4, and 0.5.

From the results presented in Figs.3 and 4, the following conclusions can be drawn:

(1) the *R* spectrum of an SDOF system with a constant damping coefficient underestimates the displacement response. The smaller the value of α is, the larger the μ value, the longer the elastic period, and the greater the underestimation will be;

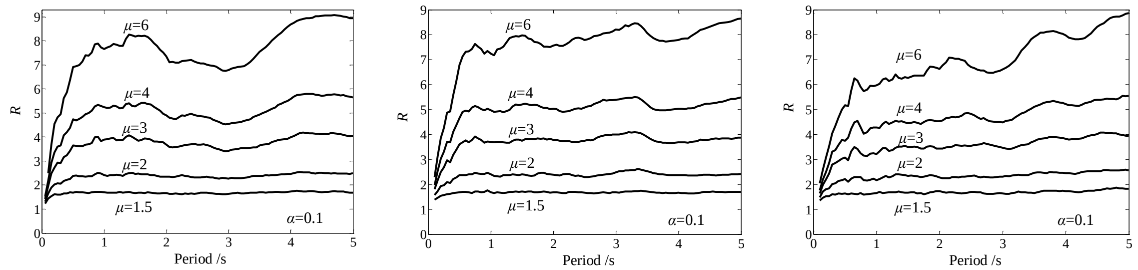

(a) R spectra, site class C (b) R spectra, site class D (c) R spectra, site class E

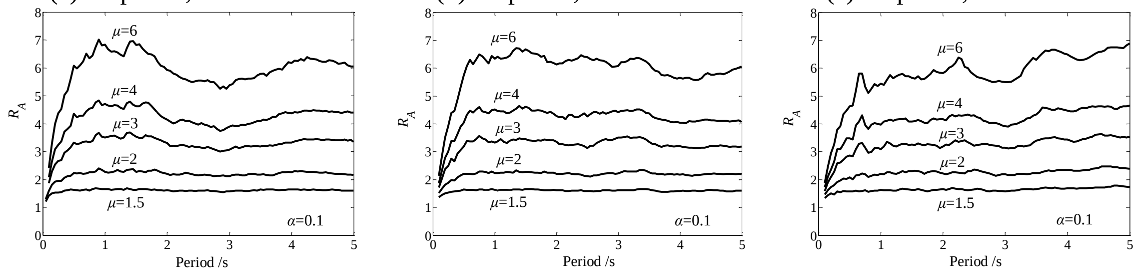

(d) R_A spectra, site class C (e) R_A spectra, site class D (f) R_A spectra, site class E

Fig. 1 The R and R_A spectra with constant ductility factors μ

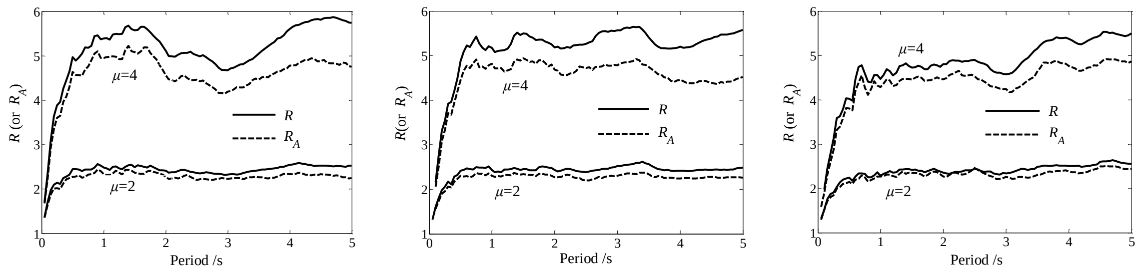

(d) R_A spectra, site class C (e) R_A spectra, site class D (f) R_A spectra, site class E

Fig. 2 Comparison of the R and R_A spectra for α = 0.2

(2) For fixed α and μ values, η shows a decreasing trend with the period T. Compared to the situation where μ is small (e.g., 1.5), this trend is not significant;

(3) At a fixed μ value, as the α value increases, the tendency of η to decrease with the increase in T gradually weakens;

(4) For a fixed α value, the larger the μ value is, the smaller the η value will be;

(5) The sites in all three classes show similar characteristics in the η spectrum;

(6) At fixed α and μ values, the softer the soil is, the larger the η value will be.

6.2 Simplified η spectrum equation

According to the above analysis, the site class has little effect on the η spectrum; therefore, the η spectra of the three sites were combined in the analysis. Based on the relationship between the combined η and α, and μ and T, a simplified expression of the η spectrum was established as follows

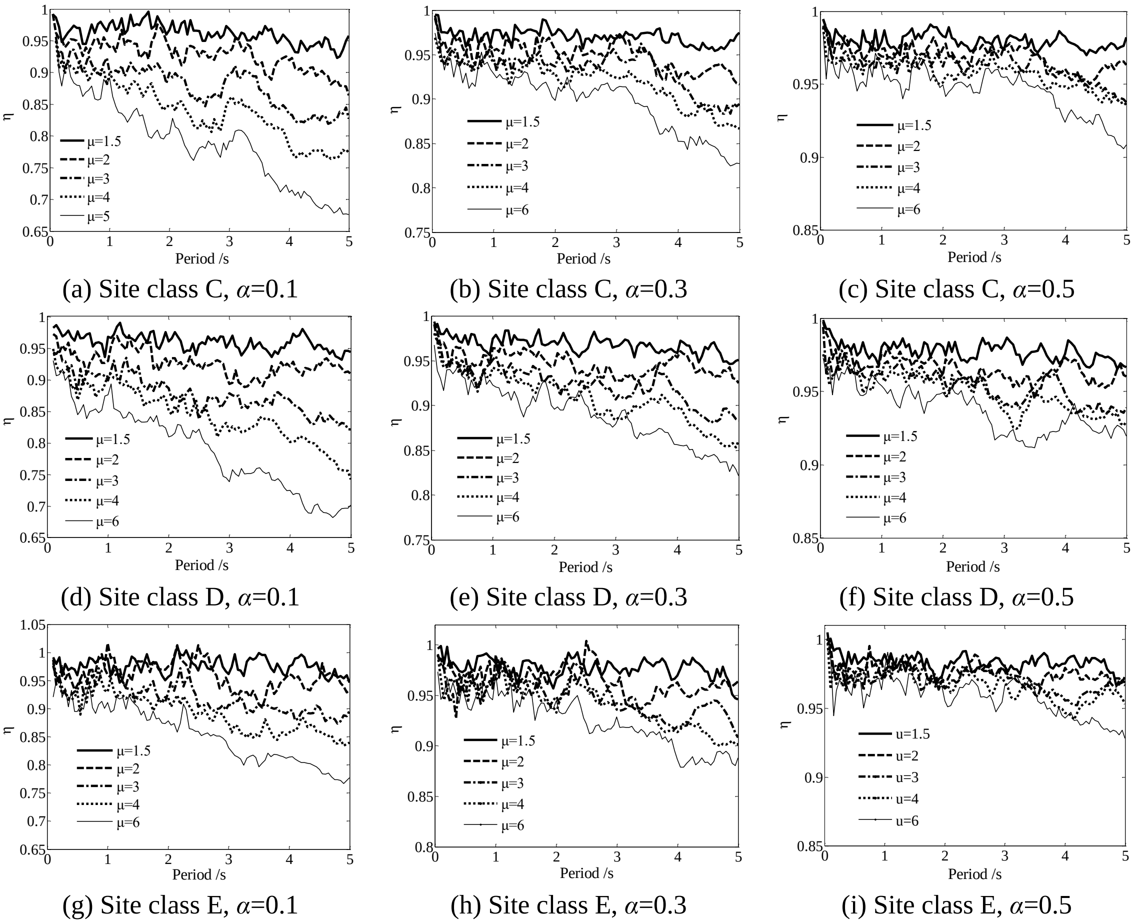

(a) Site class C, α=0.1 (b) Site class C, α=0.3 (c) Site class C, α=0.5

(d) Site class D, α=0.1 (e) Site class D, α=0.3 (f) Site class D, α=0.5

(g) Site class E, α=0.1 (h) Site class E, α=0.3 (i) Site class E, α=0.5

Fig. 3 The η spectrum with the constant ductility factors μ

Table 4 The expresssions of regression parameter b_1~b_6

Parameter	Expression	Parameter	Expression
b_1	0.00043	b_4	-0.006α+0.005
b_2	0.0217α -0.0141	b_5	0.07α-0.05
b_3	-0.0223α-0.0138	b_6	-0.067α+1.04

$$\eta\left(\alpha,\mu,T\right)=\zeta\left(\alpha,\mu\right)\cdot T+\lambda\left(\alpha,\mu\right) \tag{11}$$

$$\begin{cases}\zeta\left(\alpha,\mu\right)=b_1\mu^2+b_2\mu+b_3\\ \lambda\left(\alpha,\mu\right)=b_4\mu^2+b_5\mu+b_6\end{cases} \tag{12}$$

where the expressions of b_1~b_6 are shown in Table 4.

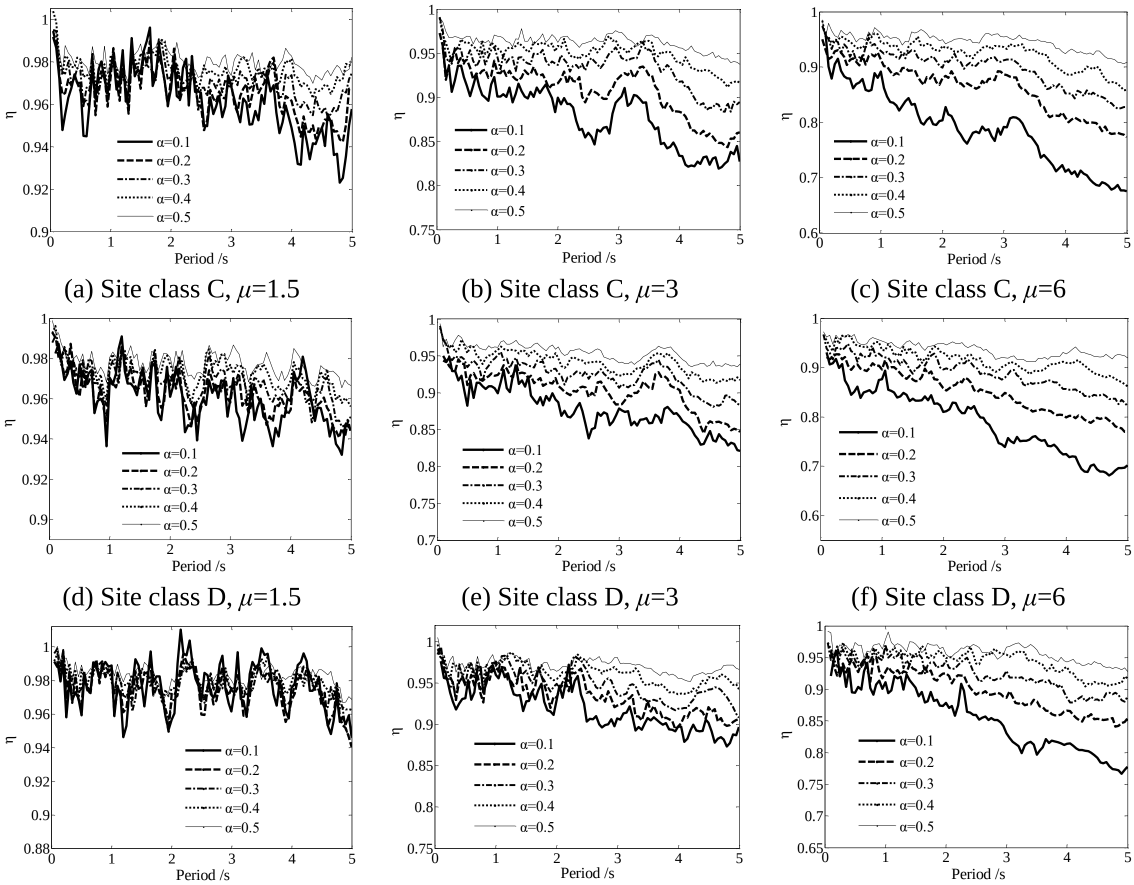

(a) Site class C, μ=1.5 (b) Site class C, μ=3 (c) Site class C, μ=6

(d) Site class D, μ=1.5 (e) Site class D, μ=3 (f) Site class D, μ=6

(g) Site class E, μ=1.5 (h) Site class E, μ=3 (i) Site class E, μ=6

Fig. 4 The η spectrum with the constant yield stiffness coefficients α

Further, to test the validity of Eqs. (11) and (12), the mean η spectrum was obtained by the time-history analysis and Eq. (11) and (12), as shown in Figs. 5 and 6. Particularly, Fig. 5 shows the comparison of the η spectra with the equivalent ductility factor for the α values of 0.1, 0.3, and 0.5. Similarly, Fig. 6 shows the comparison of the η spectra with the equivalent yield strength coefficient for the ductility factor values of 1.5, 3, and 6. Finally, the results indicated that Eqs. (11) and (12) could accurately describe the relationship between α, μ, T, and η.

7. Conclusions

Considering the limitations of the traditional strength reduction factor theory, this study proposes an SDOF system with an adaptive damping coefficient. Based on the proposed system, a modified strength reduction factor spectrum theory is established, and the equation of the η spectrum with the modification in the traditional strength reduction factor is derived.

The main research findings and conclusions of this study can be summarized as follows:

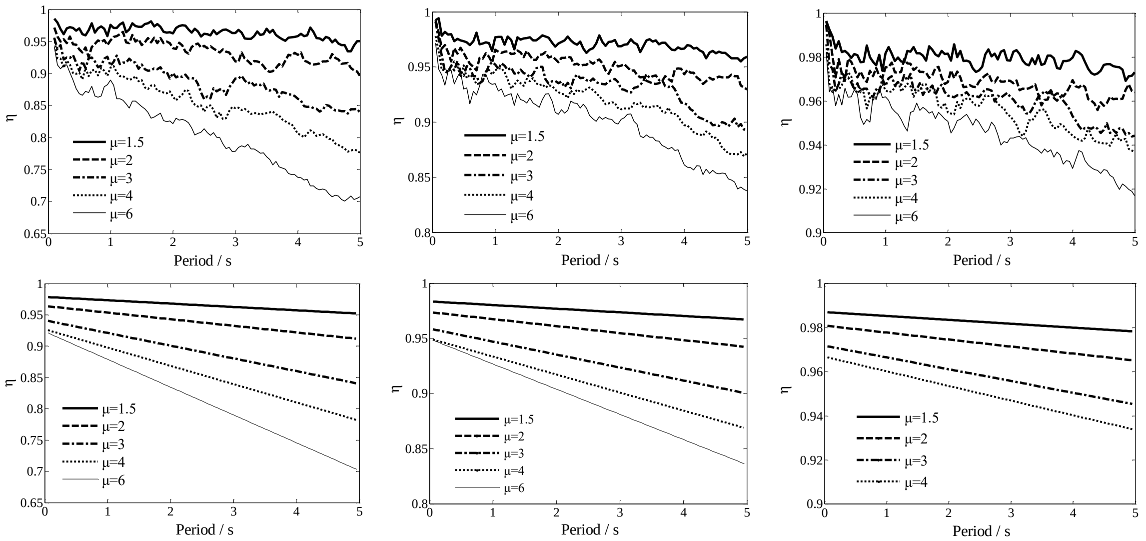

(a) α=0.1 (b) α=0.3 (c) α=0.5

Fig. 5 Comparison of the η spectra with the constant ductility factors μ

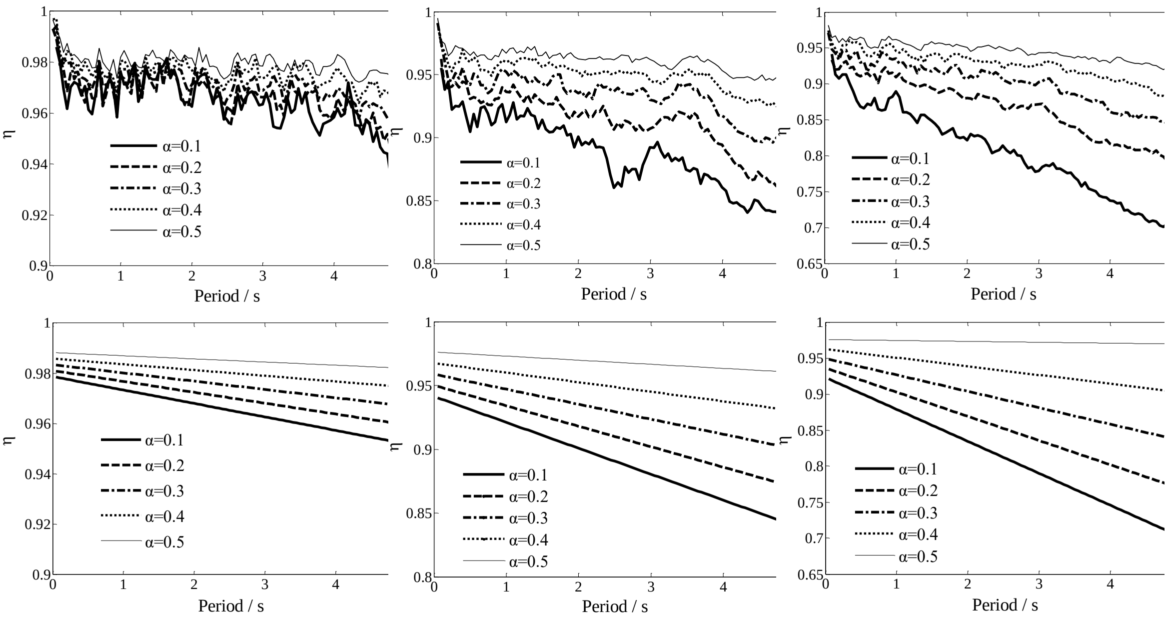

(a) μ=1.5 (b) μ=3 (c) μ=6

Fig. 6 Comparison of the η spectra with the equivalent yield strength coefficients α

(1) The R_A spectrum of equivalent SDOF systems with adaptive damping is determined. Three site classes (i.e., C, D, and E) are used in the comparison with the traditional strength reduction factor, considering a constant damping coefficient. The comparison results indicate that under the same site class, yield stiffness coefficient, and ductility factor values, the value of the strength reduction factor spectrum proposed in this study is lower than that of the traditional strength reduction factor spectrum;

(2) Parameter H is defined as the ratio of the R_A spectrum to the R spectrum. The η spectrum with an equivalent ductility factor and the mean η spectrum with an equivalent yield stiffness coefficient are obtained for the three site classes. The results show that: i) the site class has an insignificant effect on the η spectrum; ii) the yield stiffness coefficient and the ductility factor have a certain effect on the η spectrum; iii) the traditional strength reduction factor spectrum underestimates the structural displacement response, and the degree of underestimation increases as the yield stiffness coefficient decreases and the ductility factor and period increase;

(3) According to the results of the mean η spectrum, a simplified equation for the mean η spectrum is derived. The η spectrum obtained based on the history analysis is compared with that obtained by the simplified equation, and the comparison results show that the simplified η spectrum model can accurately reflect the relationships between the η spectrum and the yield stiffness coefficient, ductility factor, and T values.

Acknowledgments

The research described in this paper was financially supported by the Natural Science Foundation of China (no.51478091), the Young and Middle-aged Talents research Project of the National Ethnic Affairs Commission of China in 2019 (no: 0908210012) and the Discipline Team Project of Dalian Minzu University (no: 04442024045).

References

Ahmadi, E. and Khoshnoudian, F. (2015), “Near-fault effects on strength reduction factors of soil-MDOF structure systems”, *Soils Found.*, **55**(4), 841-856. https://doi.org/10.1016/j.sandf.2015.06.015.

Borzi, B. and Elnashai, A.S. (2000), “Refined force reduction factors for seismic design”, *Eng. Struct.*, **22**(5), 1244-1260. https://doi.org/10.1016/S0141-0296(99)00075-9.

Builidng Seismic Safety Council (2003), “NEHRP recommended provisions for seismic regulations for new buildings and other structures”, Report. FEMA-450; Federal Emergency Management Agency, Washington, D.C., USA.

Gamit, K. and Amin, J.A. (2021), “Drift and response reduction factor of RC frames designed with DDBD and FBD approach”, *J. Inst. Engineers*: *Series A*, **102**,137-151. https://doi.org/10.1007/s40030-020-00488-8.

Harikrishnan, M.G. and Gupta, V.K. (2020), “Scaling of residual displacements in terms of elastic and inelastic spectral displacements for existing SDOF systems”, *Earthq. Eng. Eng. Vib.*, **19**, 71-85. https://doi.org/10.1007/s11803-020-0548-z.

He, W.L. and Agrawal, A.K. (2004), “Pulse strength reduction factor for structures subject to near-field earthquakes”, *Structures 2004*: *Building on the Past*, *Securing the Future*, 1-8.

Kalapodis, N.A., Papagiannopoulos, G.A. and Beskos, D.E. (2018), “Modal strength reduction factors for seismic design of plane steel braced frames”, *J. Constr. Steel Res.*, **147**, 549-563. https://doi.org/10.1016/j.jcsr.2018.05.004.

Krawinkler, H. and Nassar, A.A. (1992), "Seismic design based on ductility and cumulative damage demand and capacities", *Nonlinear Seismic Analysis and Design of Reinforced Concrete Buildings*, *Applied Science*, New York, USA, 23-40.

Lee, L.H. and Han, S.W. (1999), "Determination of ductility factor considering different hysteretic models", *Earthq, Eng Struct, D,*, **28**, 957-977. https://doi.org/10.1002/(SICI)1096-9845(199909)28:9<957::AID-EQE849>3.0.CO;2-K.

Loulelis, D.G., Papagiannopoulos, G.A. and Beskos, D.E. (2018), "Modal strength reduction factors for seismic design of steel moment resisting frames", *Eng. Struct.*, **154**, 23-37. https://doi.org/10.1016/j.engstruct.2017.10.071.

Lu, Y. and Wei, J.W. (2008), "Damage-based inelastic response spectra for seismic design incorporating performance consierations", *Soil Dyn. Earthq. Eng.*, **28**, 536-549. https://doi.org/10.1016/j.soildyn.2007.08.002.

Miranda, E. and Bertero, V.V. (1994), "Evaluation of strength reduction factor for earthquake-resistance design", *Earthq. Spectra*, **l0**(2), 357-379. https://doi.org/10.1193/1.1585778.

Muho, E.V., Papagiannopoulos, G.A. and Beskos, D.E. (2018), "A seismic design method for reinforced concrete moment resisting frames using modal strength reduction factors", *Original Research*, **17**, 337-390. https://doi.org/10.1007/s10518-018-0436-3.

Newmark, N.M. and Hall, W.J. 1973), "Seismic design criteria and nuclear reactor facilities", Report No.46; Building Practices for Disaster Mitigation, National Bureau of Standard, U.S. Department of Commerce, 209-236.

Ramon, M.L., Ahmad, I.R. and Javier, S.R., Ronald, T.M., Eduardo, N.C. and Guillermo, B.L. (2022), "Assessment of strength reduction factor on concrete moment frames according to the new venezuelan seismic code", *Buildings*, **12**(3), 255. https://doi.org/10.3390/buildings12030255.

Salimbahrami, S.R. and Gholhaki, M. (2019), "Effects of higher modes and degrees of freedom (DOF) on strength feduction factor in reinforced concrete frames equipped with steel plate shear wall", *Structures*, **19**, 234-247. https://doi.org/10.1016/j.istruc.2019.01.015.

Savvinos, A., Karim, T. and Gerard, J.O. (2022), "Ground motion directionality effects on inelastic spectral displacements", Proceedings of the 3rd European Conference on Earthquake Engineering and Seismology, Bucharset, Romania, September.

Shi, Y., Wang, D.S. and Qin, H.G., Che, X., Han, J. and Zhang, Z. (2023), "Strength reduction factor spectra for SDOF systems with structural fuses", *Soil Dyn. Earthq. Eng.*, **169**, 107895. https://doi.org/10.1016/j.soildyn.2023.107895.

Silva, A.H.A., Tsiavos, A. and Stojadinovic, B. (2023), "Ductility-strength and strength-ductility relations for a constant yield dispalcement seismic design procedure", Bull. Earthq. Eng., 21, 4449-4479. https://doi.org/10.1007/s10518-023-01683-1.

Sun, L., Lv, Y. and Wei, M., Sun, H. and Zhu, J. (2020), "Shear thickening fluid based on silica with neodymium oxide nanoparticles", *Bull. Mater. Sci.*, **43**(1), 132. https://doi.org/10.1007/s12034-020-02134-2.

Thuat, D.V., Chuong, H.V. and Duong, B. (2020), "Relationship of strength reduction factor and maximum ductility factor for seismic design of one-storey industrial steel frames", *Asian J. Civil Eng.*, **21**, 841-856. https://doi.org/10.1007/s42107-020-00244-0.

Vidic, T., Fajfar, P. and Fischinger, M. (1994), "Consistent inelastic design spectra: strength and displacement", *Earthq, Eng Struct, D,*, **23**(3), 507-521. https://doi.org/10.1002/eqe.4290230504.

Wang, F., Li, H.N. and Yi, T.H. (2009), "Studies on strength reduction factor spectra of constant ductility factors for bi-directional earthquake motions", *J. Vib. Eng.*, **22**(2), 193-199. (in Chinese).

Wang, F., Li, H.N. and Zhang, C.Q. and Zhang, Y.Z. (2023), "Damage-based strength reduction factor spectra of structures subjected to bidirectional ground motions", *Adv. Struct. Eng.*, **26**(1), 72-88. https://doi.org/10.1177/13694332221119866.

Wang, F. and Li, H.N. (2014), "Research on the strength reduction factor spectra based on the superposition of bi-directional earthquake excitations", *Earthq. Eng. Eng. Dyn.*, **34**(1), 19-26. (in Chinese).

Zhang, Y.Q., Chen, J. and Sun, C.X. (2017), "Damage-based strength reduction factor for nonlinear structures subjected to sequence-type ground motions", *Soil Dyn. Earthq. Eng.*, **92**: 298-311. https://doi.org/10.1016/j.soildyn.2016.10.002.